Stretched cell cycle model for proliferating lymphocytes

Mark R. Dowling[a,b,1], Andrey Kan[a,b,1], Susanne Heinzel[a,b], Jie H. S. Zhou[a,b], Julia M. Marchingo[a,b], Cameron J. Wellard[a,b], John F. Markham[a,b,c,2], and Philip D. Hodgkin[a,b,2,3]

[a]Division of Immunology, Walter and Eliza Hall Institute of Medical Research, Parkville, VIC 3052, Australia; and [b]Department of Medical Biology, University of Melbourne, Parkville, VIC 3010, Australia; and [c]Victoria Research Laboratory, National ICT Australia, University of Melbourne, Parkville, VIC 3010, Australia

Edited by Iftach Nachman, Tel Aviv University, Tel Aviv, Israel, and accepted by the Editorial Board March 26, 2014 (received for review December 9, 2013)

Stochastic variation in cell cycle time is a consistent feature of otherwise similar cells within a growing population. Classic studies concluded that the bulk of the variation occurs in the G_1 phase, and many mathematical models assume a constant time for traversing the $S/G_2/M$ phases. By direct observation of transgenic fluorescent fusion proteins that report the onset of S phase, we establish that dividing B and T lymphocytes spend a near-fixed proportion of total division time in $S/G_2/M$ phases, and this proportion is correlated between sibling cells. This result is inconsistent with models that assume independent times for consecutive phases. Instead, we propose a stretching model for dividing lymphocytes where all parts of the cell cycle are proportional to total division time. Data fitting based on a stretched cell cycle model can significantly improve estimates of cell cycle parameters drawn from DNA labeling data used to monitor immune cell dynamics.

Smith−Martin model | FUCCI | time lapse microscopy | lognormal distribution | bromodeoxyuridine

The kinetic relationship between phases of the cell cycle first came to attention with the advent of autoradiographic techniques for detecting DNA synthesis in the 1950s (1, 2). It was realized that such data could be used to resolve the dynamics of the proliferating population if combined with an appropriate cell cycle model. However, direct filming of times to divide revealed remarkable variation, even among cloned, presumed identical, cells (3–6), eliminating simple deterministic models as the basis for cell cycle control. Working toward developing a general model, Smith and Martin made the striking observation that plotting the proportion of undivided cells versus time (so-called "alpha plots"), gave curves suggestive of two distinct phases, one relatively constant and another stochastic (7). They proposed that the two phases mapped to discrete states of the cell cycle. A resting "*A* state," they suggested, was contained within the G_1 phase from which cells could exit with constant probability per unit time (analogous to radioactive decay). The cells then entered the "*B* phase," which includes that part of G_1 not included in *A* state, as well as the entirety of $S/G_2/M$. In *B* phase, cells' activities were first described to be "deterministic, and directed towards replication," implying a constant *B* phase. However, in the same paper, this assumption was relaxed and the duration of *B* phase was described with a relatively constant random variable (7).

Although details of the quantitative relationship and biological interpretation have been debated (7–12), the rule that the bulk of kinetic variation is in G_1 phase, and that time in $S/G_2/M$ is relatively fixed, is widely accepted. Furthermore, mathematical models adopting this mechanical description (so-called "transition probability" or "compartment" models) remain popular and form the basis of many studies of lymphocyte and cancer kinetics in vitro and in vivo today (13–21).

More recently, a molecular description of cell cycle regulation, including the discovery of key regulatory proteins such as cyclins and cyclin-dependent kinases (CDKs) that initiate cyclic transition between phases, has emerged (22, 23). Despite this molecular understanding, no mechanism that would explain the stochastic, time-independent transition from *A* state to *B* phase hypothesized by Smith−Martin has been found. Furthermore, although the variation in cell cycle regulatory proteins has been well-studied at the population level (24, 25), the quantitative variation among single cells, and their role in timing the discrete cell cycle sequence, also remains largely unknown. Thus, an experimentally valid interpretation of cell cycle phases and the kinetic relationship between them suitable for building mathematical models has not been established.

An important technical aid for resolving these issues was introduced recently by Sakaue-Sawano et al., who developed a fluorescent reporter system for cell cycle phase known as Fluorescence Ubiquitination-based Cell Cycle Indicator (FUCCI) (26). In this transgenic system, a red fluorescent reporter [monomeric Kusabira-Orange 2 (mKO2)-hCdt1 (30/120)] is expressed during G_1 phase, and a green fluorescent reporter [monomeric Azami-Green (mAG)-hGem(1/110)] is then expressed from the beginning of S phase for the remainder of the cell cycle.

Here, we study the kinetics of cell cycle transitions in primary B and T lymphocytes isolated from FUCCI mice, activated in vitro using a range of stimuli to mimic the immune response. In contrast to the assumptions of the Smith−Martin and related models, time spent in both G_1 and $S/G_2/M$ phases is highly variable. We propose a model for the cell cycle of lymphocytes whereby the individual phases of the cell cycle vary in direct

Significance

Cell division is essential for an effective immune response. Estimates of rates of division are often based on DNA measurements interpreted with an appropriate model for internal cell cycle steps. Here we use time-lapse microscopy and single cell tracking of T and B lymphocytes from reporter mice to measure times spent in cell cycle phases. These data led us to a stretched cell cycle model, a novel and improved mathematical description of cell cycle progression for proliferating lymphocytes. Our model can be used to deduce cell cycle parameters for lymphocytes from DNA and BrdU labeling and will be useful when comparing the effects of different stimuli, or therapeutic treatments on immune responses, or to understand molecular pathways controlling cell division.

Author contributions: M.R.D., A.K., S.H., J.H.S.Z., J.M.M., C.J.W., J.F.M., and P.D.H. designed research; M.R.D., A.K., S.H., J.H.S.Z., J.M.M., and J.F.M. performed research; M.R.D., A.K., S.H., J.H.S.Z., J.M.M., C.J.W., J.F.M., and P.D.H. analyzed data; and M.R.D., A.K., S.H., J.H.S.Z., J.M.M., J.F.M., and P.D.H. wrote the paper.

The authors declare no conflict of interest.

This article is a PNAS Direct Submission. I.N. is a guest editor invited by the Editorial Board.

Freely available online through the PNAS open access option.

Data deposition: Implementation of computational methods and the data before numerical processing (measurements of times of cell events such as division, onset of green, etc.) is available at Github, https://github.com/johnfmarkham/mats and https://github.com/hodgkinlab/fuccipaper.

[1]M.R.D. and A.K. contributed equally to this work.

[2]J.F.M. and P.D.H. contributed equally to this work.

[3]To whom correspondence should be addressed. E-mail: hodgkin@wehi.edu.au.

This article contains supporting information online at www.pnas.org/lookup/suppl/doi:10.1073/pnas.1322420111/-/DCSupplemental.

IMMUNOLOGY

proportion to the stochastic total division time. Our "stretched cell cycle model" is qualitatively different than the Smith–Martin and related models, and suggests a common molecular mechanism controlling the time spent in all phases of the cell cycle.

Results

Temporal Profiles of FUCCI Reporter Fluorescence in Dividing Lymphocytes. To inform the development of accurate models of lymphocyte proliferation, we directly observed T and B lymphocytes isolated from FUCCI reporter mice following stimulation under different conditions. Cells were placed in microwells on the bottom of chamber slides with stimuli added to the medium (in some cases, after a period of prior stimulation in bulk cultures; see *Materials and Methods*), and filmed using a wide-field epifluorescence microscope, typically for several days. Images were recorded in bright field (to detect cell division and death), red (G_1 phase), and green ($S/G_2/M$ phases) fluorescence channels. To analyze the resulting movies, we developed a hybrid of automatic image processing techniques and manual annotation, as described in *Materials and Methods*.

Fig. 1 illustrates the major features of this analysis for B cells stimulated with the TLR9-ligand CpG-containing oligonucleotide (CpG) DNA. We previously reported that CpG-stimulated B cells do not self-adhere and can be followed through multiple generations (27). Fig. 1*A* shows frames from time-lapse imaging (movies) of a typical cell with the founder cell dividing twice, giving rise to four progeny. Fig. 1*B* illustrates the pattern of fluorescence detected using our automatic image analysis technique. As is typical for stimulation of resting lymphocytes, the first division takes much longer than subsequent rounds (27). After the first division, the two daughter cells only briefly exhibit detectable red fluorescence before both enter S phase and express increasing green fluorescence. After the second division, the four progeny appear to lose the impetus to divide (27, 28), gradually accumulate red fluorescence, and eventually either die or survive until the end of the experiment. Fig. 1*C* illustrates a stylized version of the above sequence over a single division cycle to introduce the terminology that will be used for the onset and offset of red and green fluorescence, and the features to be described under different conditions. In dividing cells, levels of red fluorescence are low, leading to noisier measurements of red on and off times (Fig. 1*B*). Hence, the time between division and offset of red fluorescence (T_{red}) is only roughly indicative of time in G_1, whereas the time between onset of green fluorescence and division (T_{grn}) is a much more reliable measure of the duration of $S/G_2/M$. Most of our conclusions are based on measurements of green fluorescence.

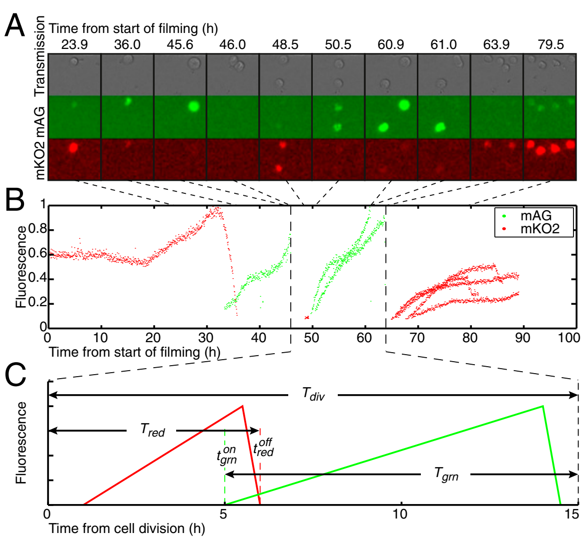

Fig. 1. Temporal profiles of FUCCI reporter fluorescence in dividing lymphocytes and schematic of the analysis method for a single division cycle. (*A*) Frames from time-lapse imaging of CpG-stimulated lymphocytes showing two division cycles followed by cessation of proliferation. (*B*) Detected normalized fluorescence in the FUCCI red and green channels using the automated method described in *Materials and Methods* and *SI Appendix, Text S5*. (*C*) Schematic of the changes in fluorescence over a single division cycle with total division time, T_{div} (judged manually by cell morphology) time from division until offset of red (mKO2) fluorescence, T_{red}, and time from the onset of green (mAG) fluorescence to the next division, T_{grn}.

The Duration of Individual Phases of the Cell Cycle are Proportional to Total Division Time. To investigate the relationship between phases of the cell cycle and total division time, we observed FUCCI lymphocytes under a range of different conditions. In addition to CpG stimulation, we also studied B cells stimulated with an αCD40 monoclonal antibody (1C10) and interleukin-4 (IL-4). CD8+ T cells were also studied—firstly from wild-type mice stimulated with the relatively weak T-cell receptor (TCR)-stimulus αCD3 (145-2C11), and interleukin-2 (IL-2). Finally, as a more physiological model of TCR ligation, we crossed the FUCCI reporter mice onto the OT-I TCR transgenic line, and stimulated CD8+ T cells from these mice with the high-affinity peptide SIINFEKL and IL-2. Single cells were observed to divide, and the two daughters were followed, if possible, for one complete division cycle until they both divided again (some cells were lost for technical reasons or due to death, and so some sibling cells are unpaired in our data sets).

Scatter plots of the duration of $S/G_2/M$ (T_{grn}) versus total division time are shown in Fig. 2. Note that each group comprises divided cells from a single division cycle. Sample means (SDs) for the total division time are as follows: 12.2 h (3.3 h) for CpG-stimulated B cells, 11.9 h (2.1 h) for αCD40/IL-4–stimulated B cells; 13.2 h (3.9 h) for αCD3/IL-2–stimulated CD8+ T cells, and 10.1 h (1.4 h) for peptide/IL-2–stimulated OT-I T cells. Importantly, for each of the stimulation conditions, there is a strong correlation between time spent in $S/G_2/M$ phases and total division time. A linear relationship passing through the origin was chosen as the simplest model. Fits allowing a straight line with a nonzero intercept are shown in *SI Appendix*, Fig. S1, and, in most cases, the 95% confidence intervals include the origin. Interestingly, $S/G_2/M$ was found to occupy the majority of total division time under all conditions—73% (71; 76) for CpG-stimulated B cells; 78% (74; 82) for αCD40/IL-4–stimulated B cells; 65% (63; 67) for αCD3/IL-2–stimulated T cells; and 72% (71; 73) for OT-I T cells—implying that G_1 occupies a small proportion of total division time (numbers in parentheses show 95% bootstrapped confidence intervals). The linear relationship was still apparent for a slowly dividing population—using a lower concentration of αCD40 for B-cell activation resulted in significantly slower division times (mean 18.2 h, SD 5.9 h), whereas the proportion of $S/G_2/M$ was unaffected, 79% (67–84%) (*SI Appendix*, Fig. S2; elsewhere in the paper, results are shown for the higher concentration only). *SI Appendix*, Fig. S3, shows the analogous plots for T_{red} (indicative of G_1) versus total division time, and *SI Appendix*, Fig. S4, shows T_{red} plotted against T_{grn}. In these plots, the positive correlations remain, although they are weaker for the rapidly dividing OT-I T cells.

Overall, these results suggest a very different picture of the cell cycle than that proposed by Smith and Martin (7). Rather than G_1 being stochastic and responsible for the majority of variation in cell cycle time with $S/G_2/M$ relatively constant, we find that both G_1 and $S/G_2/M$ occupy approximately fixed proportions of total division time. Furthermore, $S/G_2/M$ occupies the majority of division time under the conditions studied here, and is highly variable in itself and responsible for the majority of variation in division time (7, 11). We postulate that this fixed proportionality in time may apply to individual S, G_2, and M phases that cannot be directly measured by the FUCCI reporter. We refer to this model as the stretched cell cycle model.

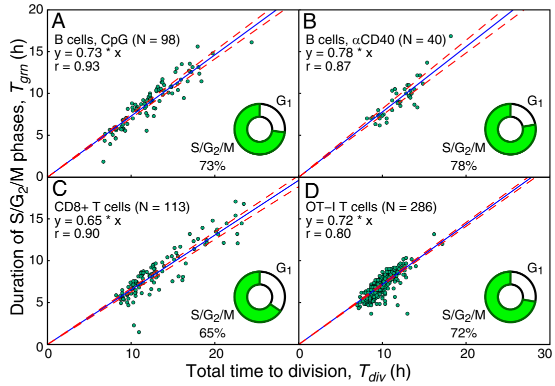

Fig. 2. Linear relationship between the total division time and the duration of the combined S/G_2/M phases for primary B and T lymphocytes responding to different stimuli. (*A*) CpG-stimulated B cells, slope = 0.73 (0.71;0.76), *r* = 0.93 (0.90;0.95). (*B*) αCD40- and IL-4–stimulated B cells, slope = 0.78 (0.74;0.82), *r* = 0.87 (0.77;0.93). (*C*) αCD3- and IL-2–stimulated CD8+ T cells, slope = 0.65 (0.63;0.67), *r* = 0.90 (0.86;0.93). (*D*) OT-I CD8+ T cells stimulated with high-affinity peptide and IL-2, slope = 0.72 (0.71;0.73), *r* = 0.80 (0.76;0.84). Solid blue lines show the fitted linear relations of the form y = (slope)*x; dashed red lines show 95% bootstrapped confidence intervals; *r* and numbers in parentheses show Pearson's correlation coefficient and 95% confidence intervals based on Fisher transformation. The slope equates to the stretching parameter for S/G_2/M used elsewhere, k_{SG2M}. The duration of the combined S/G_2/M phases (estimated as the duration of green fluorescence) appears to take approximately the same proportion (slope of the fitted line, k_{SG2M}) of the total division time within each group of cells. This proportion is schematically represented with pie charts. The linear relationship with high slope and high correlation coefficient indicates that the S/G_2/M phase occupies the majority of the cell cycle and is responsible for the majority of variation in total division time (see *SI Appendix*, Fig. S6, for direct visualization of the distributions of times in each of the phases and total division time, and comparison of sample means and SDs).

The Stretched Cell Cycle Versus Transition Probability Models. In Fig. 3 and *SI Appendix*, Fig. S5, data for lymphocyte division are presented as survival curves (Smith–Martin style alpha plots) for time in G_1 (measured as $T_{div} - T_{grn}$ rather than T_{red} for reasons described above), time in S/G_2/M (T_{grn}), and total division time (T_{div}). The plots for total division times display the characteristic minimum division time and smooth downturn leading to approximately exponential loss, noted in the earlier studies for tumor cell lines and fibroblasts (7). These total division time data can be well described by a transition probability model assuming total division time is the sum of consecutive independent exponential and Gaussian phases, *A* state and *B* phase respectively, as per the original suggestion of Smith and Martin (7) ("Exp. + Gaussian," Fig. 3 and *SI Appendix, Text 1*). Of note for the Exp. + Gaussian model, the fitted variance of the Gaussian part is comparable to the fitted variance of the exponential part (*SI Appendix*, Table S1). This contradicts the idea that most of the variation in division times is due to the exponential *A* state, and the *B* phase is relatively constant. If *B* phase is forced to be constant, as in a simplified version of the Smith–Martin model often used for mathematical convenience ("Exp. + lag"), a reasonable fit for total division times is still possible, although not as good as with a Gaussian *B* phase.

Despite these reasonable fits for total division time, predictions of the internal cell cycle phases are poor for both versions of the Smith–Martin model (Fig. 3). For Exp. + Gaussian, it makes sense to attempt to fit directly to the internal cell cycle phases, rather than total division time, but the qualitative fit is still poor (*SI Appendix*, Fig. S5). By contrast, the stretched cell cycle model assuming lognormally distributed times to divide and a single "stretching" parameter k_{SG2M} (equivalent to the slope of the fitted linear relationships in Fig. 2) for the proportion of total division time spent in S/G_2/M offers a reasonable fit for the entire alpha plot family, including the internal cell cycle phases. The stretching parameter for G_1 is calculated as $k_{G1} = 1 - k_{SG2M}$. *SI Appendix*, Fig. S6, shows the same fits when viewed as histograms of time spent in the internal phases and total division time. In the stretched model, the marginal distributions of time in G_1 and S/G_2/M will have the same shape as the division-time distribution, just scaled in time (*SI Appendix*, Text 1). A stretched model can be constructed with any distribution chosen for the total division time that fits the observed empirical distribution. In our experience, right-skewed distributions such as lognormal, gamma, and inverse Gaussian all offer relatively equivalent fits to division time data (27). *SI Appendix*, Fig. S5, includes a stretched inverse Gaussian model to illustrate this point (the fit is similar to the stretched lognormal in Fig. 3).

In summary, stretched models show a clear advantage in predicting times spent in internal phases of the cell cycle, compared with transition probability models. However, we acknowledge that practitioners in the field often use the Exp. + lag version of the Smith–Martin model for reasons of analytic or computational convenience. In such cases, a minimally disruptive change would be to keep the Exp. + lag model for total division time, but simply add a stretching parameter for internal phases. *SI Appendix*, Fig. S5, illustrates that this change does indeed improve the estimate of time spent in the internal phases, although the fit is still not as good as other two-parameter right-skewed distributions such as lognormal or inverse Gaussian.

IMMUNOLOGY

Estimating the Proportion of Division Time Spent in S and G_2/M Cell Cycle Phases. We were interested in whether the stretching observation held true for the S, G_2, and M phases individually. The S phase cannot be separated using the FUCCI reporter alone.

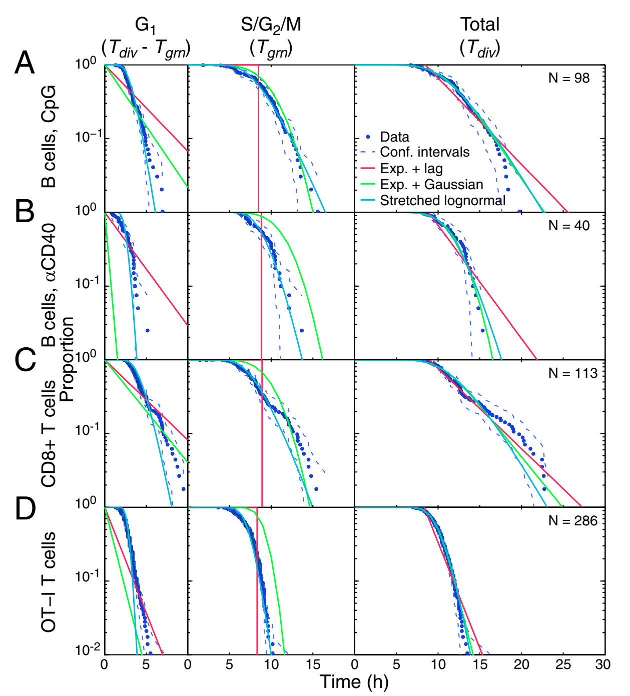

Fig. 3. Alpha plots (empirical tail distributions) for estimated times spent in G_1 phase (*Left*), S/G_2/M phases (*Center*) and total division times (*Right*) overlaid with fitted models for different experiments. (*A*) CpG-stimulated B cells. (*B*) αCD40- and IL-4–stimulated B cells. (*C*) αCD3- and IL-2–stimulated CD8+ T cells. (*D*) OT-I CD8+ T cells stimulated with high-affinity peptide and IL-2. Lag-exponential, exponentially modified Gaussian (Smith and Martin model), and stretched lognormal models were defined and fitted as explained in *SI Appendix, Text 1*. The data points are a Kaplan–Meier estimate of the empirical survival curve, and the dashed lines indicate 95% confidence intervals calculated using Greenwood's formula. In each plot, one to three data points below 0.01 on the vertical axis are not shown (*SI Appendix, Text 6*).

Instead, we noted that it was possible to separate cells into G_1, S, and G_2/M subpopulations by flow cytometry by combining bromodeoxyuridine (BrdU) pulse labeling and direct staining of DNA with 7-amino-actinomycin D (7AAD) (*SI Appendix*, *Text 2* and Fig. S7). We sought evidence for stretching S and G_2/M phases of the cell cycle individually, by considering the effect of varying the length of the BrdU pulse on the relative size of BrdU[negative (–ve)] DNA(×2) population. For short pulses, this population corresponds to cells in G_2/M. As the pulse length becomes longer, cells that were in G_2/M at the start of the pulse will divide and halve their DNA, becoming DNA(×1). Conversely, some cells in S phase at the start of the pulse will now be detected as BrdU[positive (+ve)] even once they enter G_2/M. The overall effect is that the BrdU(−ve) DNA(×2) population reduces as the length of the pulse increases. This effect is illustrated in the time course of flow cytometry plots in Fig. 4*A*.

We then developed a mathematical model for analyzing the BrdU(−ve) DNA(×2) population. This model is based on previous work, where we derived an expression for the joint distribution of total division time, T_{div}, and remaining time until next division, δ, within an asynchronous and exponentially growing population of cells (29). When supplemented with a further assumption about the duration of S phase, T_S, this model can be used to calculate the proportion of cells found to be BrdU(−ve) DNA(×2), $p(l)$, as a function of pulse length, l. The full mathematical details of this model are described in *SI Appendix*, *Text 3*, and Fig. 4*B* is a schematic introducing the parameters relevant for the model.

One of the assumptions of our model is that cells are in an exponential growth phase with negligible death. Therefore, we chose CpG-stimulated B cells (day 2) and αCD3- and IL-2–stimulated T cells (day 3) to fit the model to, as they are as close as possible to these conditions based on flow cytometry. The cells were also stained with the division-tracking dye CellTrace Violet (CTV), to exclude undivided cells from the analysis. The mean and SD of total division time and the stretching parameter for S/G_2/M were fixed from the filming data described in Fig. 2. We considered two options for describing the duration of the S and G_2/M phases with one additional free parameter—either stretched S [$T_S = k_S \cdot T_{div}$, $T_{G2M} = (k_{SG2M} - k_S) \cdot T_{div}$, k_S free] or constant S ($T_{G2M} = k_{SG2M} \cdot T_{div} - T_S$, T_S free). These models were fit to the data, producing the results illustrated in Fig. 4 *C* and *D*. As can be seen, with the stretched S assumption, the fits are close, and qualitatively follow the shape of the real data, demonstrating consistency with the stretching hypothesis. By contrast, with constant S, the fits are noticeably poorer for both data sets. In the stretched model, as the S/G_2/M proportion was already known from the FUCCI filming data, we estimate the proportion of time spent in G_1, S, and G_2/M phases of the total division time as, for B cells, 0.27 (0.24;0.29), 0.57 (0.55;0.60), and 0.16 (0.16;0.16), and for T cells, 0.35 (0.33;0.37), 0.51 (0.48;0.53), and 0.14 (0.14;0.15), respectively (Fig. 4 *C* and *D*). Although these model-based conclusions cannot be taken as definitive proof that the S and G_2/M phases stretch individually, consistency of the model with DNA labeling methods may lead to improved predictions and interpretation of such data in future.

Cell Cycle Phases Are Highly Correlated in Sibling Cells. Returning to our filming data, we investigated sibling correlations in progression through the cell cycle, to provide further insight into the underlying mechanism of cell cycle stretching. Fig. 5 *A*–*D* shows bar graphs for each of the cell/stimulation conditions, where the left-hand bars represent the times spent in different phases for one sibling, rank ordered by total division time, and the right-hand bars represent the corresponding sibling. The relatively faithful mirroring illustrates a high degree of sibling correlation. Fig. 5 *E*–*H* shows the same data, with the phases in each cell scaled according to total division time. The horizontal line below each condition represents progression throughout the cell cycle, and the histograms above and below show the distribution over times of events (on and off for red and green fluorescence)

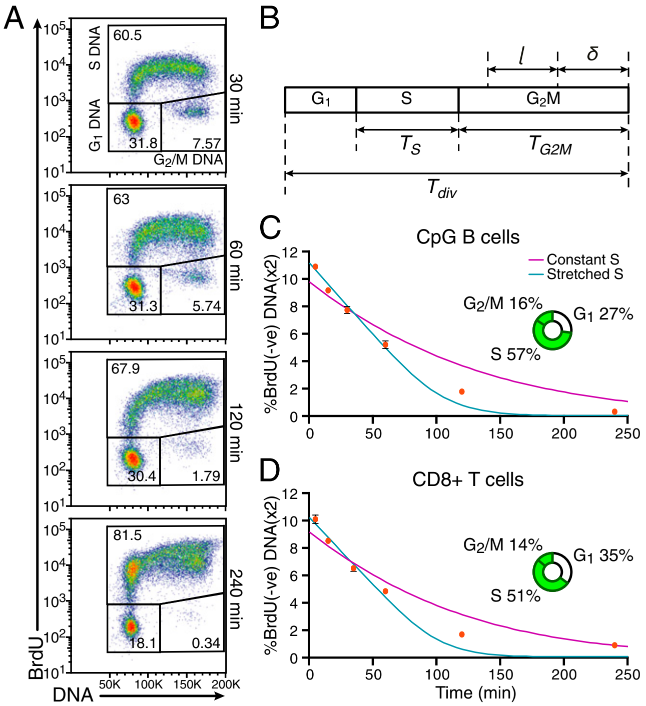

Fig. 4. DNA labeling with BrdU and direct staining with 7AAD in proliferating lymphocytes, and fitting with the stretched and constant S-phase models. (*A*) Flow cytometry plots of BrdU versus DNA for different lengths of BrdU pulse to CpG-stimulated B cells showing that the BrdU(−ve) DNA(×2) population diminishes with increasing pulse length. (*B*) Schematic establishing notation for the mathematical modeling described in detail in *SI Appendix, Text 3*. Here T_{div} is the total division time, T_S is the time spent in S, T_{G2M} is the time spent in G_2/M, δ is the remaining division time, and l is the BrdU pulse length. (*C* and *D*) Percentages BrdU(−ve) DNA(×2) as a function of BrdU pulse length for CpG-stimulated B cells (*C*) or αCD3- and IL-2–stimulated CD8+ T cells (*D*), with fits of mathematical models described in text and *SI Appendix, Text 3*. Means are shown with error bars indicating ±SE in the mean (SEM) of three replicate wells (note that for some points, the error bars are so small that they are not visible by eye).

among all cells. *SI Appendix*, Fig. S8, quantifies the degree of correlation further. *SI Appendix*, Fig. S8*C*, are scatter plots of total division times for the two siblings, showing strong correlations, as expected from previous studies (27). *SI Appendix*, Fig. S8 *A* and *B*, shows that these correlations are also present in the time to offset of red fluorescence and the duration of S/G_2/M part for siblings. Overall, these results imply that the processes governing variation in both division time and the different phases of the cell cycle are heritable and strongly shared by siblings.

Discussion

Mathematical models of cell cycle progression that attempt to describe and explain the striking and consistent division time heterogeneity seen within populations of similar cells have a long history (7–9, 11, 12, 21, 30). The use of FUCCI reporter and time lapse microscopy imaging allowed us to directly measure the duration of different phases of the cell cycle and test the underlying assumptions of the influential transition probability models first proposed by Smith and Martin (7). We have focused on proliferating lymphocytes activated in various ways, as this is a common scenario for which Smith–Martin type models are currently used (13, 14, 16). Several features of our data argue against this class of models (Fig. 3 and *SI Appendix*, Figs. S5 and S6 and *Texts 1* and *4*). Most strikingly, the duration of the combined S/G_2/M phases is highly variable within the cell population and, in fact, is responsible for the majority of variation in total division time. This is in stark contrast to the original idea

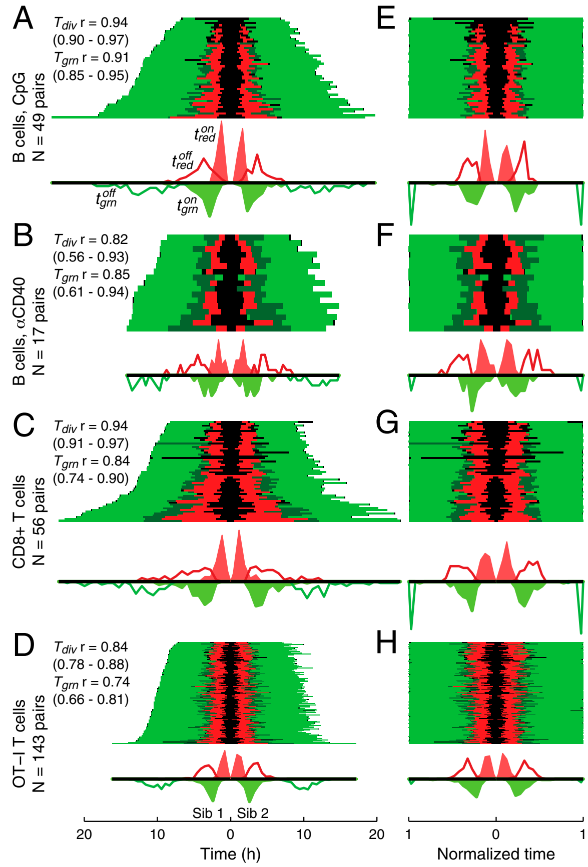

Fig. 5. Cell cycle phases are highly correlated in sibling cells. Bars represent total times to divide for sibling cells (left- and right-hand sides), and colors show temporal location of red fluorescence (red), green fluorescence (green), both (dark green), or none (black). The durations are shown either in hours (*A–D*) or relative to the total time to divide (*E–H*) for B cells, CpG (*A* and *E*), B cells, αCD40 (*B* and *F*), CD8+ T cells (*C* and *G*), and OT-I T cells (*D* and *H*) The histograms under each group of bars show the distributions of times to onset of red (filled red curves), offset of red (red lines), onset of green (filled green curves), and offset of green (green lines) for corresponding groups of cells.

behind transition probability models, where these phases were thought to take a constant (or nearly so) time, and cell-to-cell variability arose primarily due to variation within the G_1 phase. Furthermore, we found strong correlations between the duration of G_1 phases in siblings, whereas the Smith and Martin model does not expect the duration of sibling G_1 phases to be strongly correlated (10). Instead, our data suggest a qualitatively different, and surprisingly simple, manner of connecting phases of the cell cycle. In our model, all parts of the cell cycle lengthen and shorten in proportion to the total division time of the cell. Hence, we call this model the stretched cell cycle model.

Taken together, our results demonstrate that a shared and heritable factor affects progression through all parts of the cell cycle. The molecular mechanism underlying these observations is clearly of great interest. Candidates for controlling changes in rates include quantitative levels of known cell cycle regulatory proteins such as cyclins or CDKs, which can be passed on to daughter cells, along with epigenetic changes controlling the rate of mRNA synthesis. In the case of CDKs, a mechanism has already been proposed that would produce a stretching effect based on studies in yeast. In these cells, entry to both S and M phases of the cell cycle can be triggered by increasing thresholds of the same CDK (24, 25, 31). Thus, heritable, epigenetic variation in the rate of accumulation of such factor(s) would lead to sibling cells with a range of times to each event, and a strong mechanistic connection between times to S, and times to M phase in individual cells.

The mathematical assumptions of the stretched model may also require further development to explain all of the observed features of the data. For example, in this study, we assumed a fixed proportion of time was spent in different cell cycle phases, and this was able to explain the data in Fig. 2 well (near-linear relationships, Pearson's r = 0.8–0.93). However, there is clearly still some variation about the straight line that can be explained by measurement noise, but can also suggest that the stretching proportion may vary slightly on a cell-to-cell basis. We also cannot rule out the possibility that there is a relatively short part of cell cycle that does not stretch. For example, *SI Appendix*, Fig. S1, demonstrates that the data are consistent with a nonzero intercept (nonstretched period) of the order of 1–2 h in duration. Whether this nonstretched period is indeed present, and whether there is any biological significance, remains unknown.

Finally, the FUCCI reporter combined with the stretched cell cycle model opens up many experimental possibilities for studies of cell kinetics and differentiation in other cell types. The lymphocytes we have studied here are undergoing a series of divisions, and are not expected to pass through a quiescent (G_0) phase. It will be interesting to determine if cell cycle stretching holds across different cell types and stimulation conditions, in vivo as well as in vitro, and could thereby be adopted as a generalized model. If so, the implications for interpreting a range of common experimental techniques, including BrdU incorporation and DNA labeling, may potentially lead to new insights into cell cycle regulation in normal and transformed cells.

Materials and Methods

Mice. All mice were maintained under specific pathogen-free conditions and used between 5 and 12 wk of age. All animal experiments were performed under the approval of the Walter and Eliza Hall Institute (WEHI) Animal Ethics Committee. C57BL/6 mice were obtained from the WEHI animal facility. All transgenic mice used were on a C57BL/6 background. FUCCI RG mice were constructed by crossing FUCCI Red (B6.B6D2-Tg(FUCCI)596Bsi) with FUCCI Green (B6.B6D2-Tg(FUCCI)504Bsi) mice, both obtained from the Riken BioResource Centre (26). In one experiment (αCD40/IL-4 stimulation of B cells), FUCCI-RG crossed to CAG-ECFP (32) were used, although the cyan fluorescence was not filmed. To obtain OT-I-FUCCI RG mice, OT-I mice expressing T-cell receptors specific for chicken ovalbumin (obtained from WEHI animal facilities) were crossed with FUCCI RG mice.

Cell Preparation and in Vitro Cell Culture. Bulk culture of B or T cells before filming was done in lymphocyte culture medium made of advanced RPMI-1640 supplemented with 5% (vol/vol) FBS, 10 mM Hepes, 100 U/mL penicillin, 100 μg/mL streptomycin, 1x GlutaMAX (all Invitrogen), and 50 μM β-2-mercaptoethanol (Sigma). For microscopy, cells were cultured in filming medium made of advanced RPMI 1640 without phenol red, and supplemented as for bulk culture. For B-cell stimulations, small resting B cells were isolated using established protocol (30) with a discontinuous Percoll (GE Healthcare) gradient and negative magnetic bead isolation kit (B-cell isolation kit, Miltenyi Biotech). Purity was typically >95% (B220+ CD19+). B cells were stimulated either with 3 μM CpG 1668 (sequence 5′-TCCATGACGTTCCTGATGCT-3′, Geneworks) or with 40 μg/mL (unless otherwise stated) αCD40 (clone 1C10, WEHI monoclonal antibody facility) and 1000 U/mL IL-4 (baculovirus-transfected Sf21 insect cell supernatant, WEHI). For CpG stimulation, cells were resuspended in filming medium in the presence of CpG at 7000 cells per mL. Then 250 μL per chamber were placed into chamber slides (μ-Slide 8 well, Ibidi) containing 250-μm microgrids (MGA-250-01, Daniel Day, Microsurfaces) and incubated at 37 °C with 5% CO_2 in a humidified atmosphere for 22 h before commencement of filming. For αCD40/IL4 stimulations, cells were labeled with 7.5 μM CTV (Invitrogen) according to the manufacturer's instructions, resuspended in lymphocyte culture medium containing αCD40 and IL-4, and cultured at 4×10^5 cells per mL for 4 d. Cells were then harvested, and sorted from division 4 based on the dilution of division tracking dye CTV using a BD FACSAria. Sorted cells were resuspended at 5×10^4 cells per mL in filming medium supplemented with αCD40 and IL-4 as before, and 250 μL added to a μ-slide chamber containing a 50-μm microgrid (MGA-050-01, Microsurfaces) for filming.

CD8+ T cells were isolated from lymph nodes of C57BL/6 or OT-I mice using the CD8a+ T Cell Isolation Kit II (Miltenyi Biotech). Purity was typically between 85% and 95% (CD8+ for C57BL/6, or CD8+Vα2+ for OT-I). C57BL/6 CD8+ T cells were stimulated at 2×10^5 cells per mL in 1-mL cultures in a 24-well plate precoated with 10 μg/mL αCD3 antibody (clone 145-2C11) in filming medium in the presence of 100 U/mL murine IL-2 (a gift from G. Zurawski, DNAX Research Institute of Molecular and Cellular Biology). Cells were harvested after 24 h and 250 μL per chamber placed into μ-Slide 8 well chamber slides containing 50-μm microgrids for filming. OT-I CD8+ T cells were labeled with 5 μM CTV, stimulated with 0.01 μg/mL SIINFEKL peptide (Auspep) in lymphocyte culture medium in the presence of 31.6 U/mL human IL-2 (Peprotech), and cultured at 10^5 cells per well in 96-well U-bottom plates. After 24 h, cells were harvested, washed, resuspended at 5×10^4 cells per mL in filming medium containing 31.6 U/mL human IL-2 and 25 μg/mL antimouse IL-2 antibody (made from hybridoma cell line S4B6)—to block endogenous IL-2 production and ensure IL-2 remained constant throughout the experiment—and 250 μL per chamber placed into μ-Slide 8 well chamber slides for filming. Cell densities were chosen such that a significant proportion of microwells contained only one cell after settling.

BrdU Labeling and DNA Content Analysis. B cells or CD8+ T cells were isolated from FUCCI-green mice as described above. B cells were stimulated with 3 μM CpG for 2 d or with 10 μg/mL αCD40 and 1000 U/mL IL-4 for 3 d. CD8+ T cells were stimulated in the presence of 100 U/mL IL-2 in a 24-well plate precoated with 10 μg/mL αCD3 for 3 d. At the end of the culture, 10 μM BrdU was added to each well for the times indicated. BrdU incorporation and DNA content were analyzed using the APC BrdU flow Kit (BD Biosciences) following the manufacturer's protocol. Gates to determine percentages of cells in G_1, S, or G_2/M phases were based on contour plots. Triple replicates were analyzed for each condition, and time point and results are shown as mean $\pm$SEM.

Live-Cell Microscopy and Image Processing. The chamber slide containing cells sorted from different divisions was transferred to an environment-controlled [37 °C, 5% (vol/vol) CO_2, humidified] Zeiss Axiovert 200M microscope. A Zeiss Plan-Apochromat 20× objective (n.a. 0.8) was used, and fluorescence and bright-field images were captured with a Zeiss AxioCam MRm (1.4 megapixels) attached via a 0.6× c-mount. The light source was a Zeiss Colibri module fitted with 490-nm and 565-nm beam splitters, as well as 540- to 580-nm and 470-nm light-emitting diodes, which were used to excite mKO2 and mAG, respectively. One of two filter set combinations was used. For the CpG experiment, Zeiss Filter Set 13 (excitation 470/20, Dichroic 495, emission 505–530) was used for mAG and Zeiss Filter Set 45 (excitation 560/40, Dichroic 585, emission 630/75) was used for mKO2. For all of the other experiments, the Brightline LF405/488/561/635-A-ZHE filter set (Semrock) was used for both fluorophores. Microscopy parameters for each experiment are shown in *SI Appendix, Text 5*.

Unless otherwise stated, all of the image processing was implemented using the software package Microgrid Array Tools running under Matlab 2012a. Image processing is described in detail in *SI Appendix, Text 5*. The package is available at https://github.com/johnfmarkham/mats.

Mathematical Modeling. Details of mathematical modeling are presented in *SI Appendix, Texts 1* and *3*. Relevant source code and data can be downloaded from https://github.com/hodgkinlab/fuccipaper.

ACKNOWLEDGMENTS. We thank Carel van Gend, Ken Duffy, Tom Weber, and Edwin Hawkins for discussion and comments on the manuscript; Kelly Rogers, Karl Dudfield, Rajib Chakravorty, David Rawlinson, and Alan Zhang for assistance in establishing long-term microscopy and developing image processing routines; Lynn Corcoran for help with methods; and Dave Tarlinton for help with mouse breeding. FUCCI Red and FUCCI Green mice were provided by the Riken BioResource Centre through the National BioResource Project of the Ministry of Education, Culture, Sports, Science and Technology-Japan. This work was supported by the National Health and Medical Research Council via project Grant 1010654, program Grant 1016647, and fellowships to M.R.D. and P.D.H. as well as Independent Research Institutes Infrastructure Support Scheme Grant 361646. We also received support from the Victorian State Government Operational Infrastructure scheme and National ICT, Australia (NICTA). NICTA is funded by the Australian Government as represented by the Department of Broadband, Communications and the Digital Economy and the Australian Research Council through the ICT Centre of Excellence program. J.H.S.Z. and J.M.M. are the recipients of an Australian Postgraduate Award.

1. Howard A, Pelc SR (1951) Nuclear incorporation of P-32 as demonstrated by autoradiographs. *Exp Cell Res* 2(2):178–187.
2. Steel GG (1986) Autoradiographic analysis of the cell cycle: Howard and Pelc to the present day. *Int J Radiat Biol Relat Stud Phys Chem Med* 49(2):227–235.
3. Killander D, Zetterberg A (1965) Quantitative cytochemical studies on interphase growth. I. Determination of DNA, RNA and mass content of age determined mouse fibroblasts in vitro and of intercellular variation in generation time. *Exp Cell Res* 38(2): 272–284.
4. Dawson KB, Madoc-Jones H, Field EO (1965) Variations in the generation times of a strain of rat sarcoma cells in culture. *Exp Cell Res* 38(1):75–84.
5. Marin G, Bender MA (1966) Radiation-induced mammalian cell death: Lapse-time cinemicrographic observations. *Exp Cell Res* 43(2):413–423.
6. Terasima T, Tolmach LJ (1963) Growth and nucleic acid synthesis in synchronously dividing populations of HeLa cells. *Exp Cell Res* 30(2):344–362.
7. Smith JA, Martin L (1973) Do cells cycle? *Proc Natl Acad Sci USA* 70(4):1263–1267.
8. Shields R, Brooks RF, Riddle PN, Capellaro DF, Delia D (1978) Cell size, cell cycle and transition probability in mouse fibroblasts. *Cell* 15(2):469–474.
9. Castor LN (1980) A G1 rate model accounts for cell-cycle kinetics attributed to 'transition probability.' *Nature* 287(5785):857–859.
10. Minor PD, Smith JA (1974) Explanation of degree of correlation of sibling generation times in animal cells. *Nature* 248(445):241–243.
11. Shields R (1977) Transition probability and the origin of variation in the cell cycle. *Nature* 267(5613):704–707.
12. Brooks RF, Bennett DC, Smith JA (1980) Mammalian cell cycles need two random transitions. *Cell* 19(2):493–504.
13. De Boer RJ, Perelson AS (2013) Quantifying T lymphocyte turnover. *J Theor Biol* 327: 45–87.
14. Ganusov VV, Milutinović D, De Boer RJ (2007) IL-2 regulates expansion of CD4+ T cell populations by affecting cell death: Insights from modeling CFSE data. *J Immunol* 179(2):950–957.
15. Golubev A (2012) Transition probability in cell proliferation, stochasticity in cell differentiation, and the restriction point of the cell cycle in one package. *Prog Biophys Mol Biol* 110(1):87–96.
16. Lee HY, Perelson AS (2008) Modeling T cell proliferation and death in vitro based on labeling data: Generalizations of the Smith−Martin cell cycle model. *Bull Math Biol* 70(1):21–44.
17. Lee TJ, Yao GA, Bennett DC, Nevins JR, You LC (2010) Stochastic E2F activation and reconciliation of phenomenological cell-cycle models. *PLoS Biol* 8(9):e1000488.
18. León K, Faro J, Carneiro J (2004) A general mathematical framework to model generation structure in a population of asynchronously dividing cells. *J Theor Biol* 229(4): 455–476.
19. Luzyanina T, et al. (2007) Computational analysis of CFSE proliferation assay. *J Math Biol* 54(1):57–89.
20. Macklin P, Edgerton ME, Thompson AM, Cristini V (2012) Patient-calibrated agent-based modelling of ductal carcinoma in situ (DCIS): From microscopic measurements to macroscopic predictions of clinical progression. *J Theor Biol* 301:122–140.
21. Zilman A, Ganusov VV, Perelson AS (2010) Stochastic models of lymphocyte proliferation and death. *PLoS ONE* 5(9):e12775.
22. Nurse P (2000) A long twentieth century of the cell cycle and beyond. *Cell* 100(1): 71–78.
23. Nurse P, Masui Y, Hartwell L (1998) Understanding the cell cycle. *Nat Med* 4(10): 1103–1106.
24. Oikonomou C, Cross FR (2011) Rising cyclin-CDK levels order cell cycle events. *PLoS ONE* 6(6):e20788.
25. Sorrell DA, Combettes B, Chaubet-Gigot N, Gigot C, Murray JAH (1999) Distinct cyclin D genes show mitotic accumulation or constant levels of transcripts in tobacco bright yellow-2 cells. *Plant Physiol* 119(1):343–352.
26. Sakaue-Sawano A, et al. (2008) Visualizing spatiotemporal dynamics of multicellular cell-cycle progression. *Cell* 132(3):487–498.
27. Hawkins ED, Markham JF, McGuinness LP, Hodgkin PD (2009) A single-cell pedigree analysis of alternative stochastic lymphocyte fates. *Proc Natl Acad Sci USA* 106(32): 13457–13462.
28. Turner ML, Hawkins ED, Hodgkin PD (2008) Quantitative regulation of B cell division destiny by signal strength. *J Immunol* 181(1):374–382.
29. Dowling MR, Milutinović D, Hodgkin PD (2005) Modelling cell lifespan and proliferation: Is likelihood to die or to divide independent of age? *J R Soc Interface* 2(5): 517–526.
30. Hawkins ED, Turner ML, Dowling MR, van Gend C, Hodgkin PD (2007) A model of immune regulation as a consequence of randomized lymphocyte division and death times. *Proc Natl Acad Sci USA* 104(12):5032–5037.
31. Uhlmann F, Bouchoux C, López-Avilés S (2011) A quantitative model for cyclin-dependent kinase control of the cell cycle: Revisited. *Philos Trans R Soc Lond B Biol Sci* 366(1584):3572–3583.
32. Hadjantonakis AK, Macmaster S, Nagy A (2002) Embryonic stem cells and mice expressing different GFP variants for multiple non-invasive reporter usage within a single animal. *BMC Biotechnol* 2(1):11.